Positron bunching and electrostatic transport system for the production and emission of dense positronium clouds into vacuum

S. Aghion, C. Amsler, A. Ariga, T. Ariga, A.S. Belov, G. Bonomi, P. Bräunig, J. Bremer, R.S. Brusa, L. Cabaret, et al.

HAL Id: in2p3-01258082
https://hal.in2p3.fr/in2p3-01258082

Submitted on 18 Jan 2016

Positron bunching and electrostatic transport system for the production and emission of dense positronium clouds into vacuum

S. Aghion [a,b], C. Amsler [c], A. Ariga [c], T. Ariga [c], A.S. Belov [d], G. Bonomi [e,f], P. Bräunig [g], J. Bremer [h], R.S. Brusa [i,j], L. Cabaret [k], M. Caccia [b,l], R. Caravita [h,m,n], F. Castelli [b,o], G. Cerchiari [p], K. Chlouba [q], S. Cialdi [b,o], D. Comparat [k], G. Consolati [a,b], A. Demetrio [g], L. Di Noto [m,n], M. Doser [h], A. Dudarev [h], A. Ereditato [c], C. Evans [a,b], J. Fesel [h], A. Fontana [f], O.K. Forslund [h], S. Gerber [h], M. Giammarchi [b,c], A. Gligorova [r], S. Gninenko [d], F. Guatieri [i,j], S. Haider [h], H. Holmestad [s], T. Huse [s], I.L. Jernelv [h], E. Jordan [p], T. Kaltenbacher [c], A. Kellerbauer [p], M. Kimura [c], T. Koetting [h], D. Krasnicky [n], V. Lagomarsino [m,n], P. Lebrun [w], P. Lansonneur [w], S. Lehner [t], J. Liberadzka [h], C. Malbrunot [h,t], S. Mariazzi [t,*], L. Marx [h], V. Matveev [d,u], Z. Mazzotta [b,o], G. Nebbia [v], P. Nedelec [w], M. Oberthaler [g], N. Pacifico [r], D. Pagano [e,f], L. Penasa [i,j], V. Petracek [q], C. Pistillo [c], F. Prelz [b], M. Prevedelli [x], L. Ravelli [i,j], B. Rienäcker [h], O.M. Røhne [s], S. Rosenberger [h], A. Rotondi [f,y], M. Sacerdoti [o], H. Sandaker [s], R. Santoro [b,l], P. Scampoli [c,z], F. Sorrentino [n], M. Spacek [q], J. Storey [c], I.M. Strojek [q], G. Testera [n], I. Tietje [h], S. Vamosi [t], E. Widmann [t], P. Yzombard [k], S. Zavatarelli [n], J. Zmeskal [t], (AEgIS Collaboration)

[a] Politecnico of Milano, Piazza Leonardo da Vinci 32, 20133 Milano, Italy
[b] INFN Milano, via Celoria 16, 20133 Milano, Italy
[c] Laboratory for High Energy Physics, Albert Einstein Center for Fundamental Physics, University of Bern, 3012 Bern, Switzerland
[d] Institute for Nuclear Research of the Russian Academy of Science, Moscow 117312, Russia
[e] Department of Mechanical and Industrial Engineering, University of Brescia, via Branze 38, 25123 Brescia, Italy
[f] INFN Pavia, via Bassi 6, 27100 Pavia, Italy
[g] Kirchhoff-Institute for Physics, Heidelberg University, Im Neuenheimer Feld 227, 69120 Heidelberg, Germany
[h] Physics Department, CERN, 1211 Geneva 23, Switzerland
[i] Department of Physics, University of Trento, via Sommarive 14, 38123 Povo, Trento, Italy
[j] TIFPA/INFN Trento, via Sommarive 14, 38123 Povo, Trento, Italy
[k] Laboratoire Aimé Cotton, Université Paris-Sud, ENS Cachan, CNRS, Université Paris-Saclay, 91405 Orsay Cedex, France
[l] Department of Science, University of Insubria, Via Valleggio 11, 22100 Como, Italy
[m] Department of Physics, University of Genova, via Dodecaneso 33, 16146 Genova, Italy
[n] INFN Genova, via Dodecaneso 33, 16146 Genova, Italy
[o] Department of Physics, University of Milano, via Celoria 16, 20133 Milano, Italy
[p] Max Planck Institute for Nuclear Physics, Saupfercheckweg 1, 69117 Heidelberg, Germany
[q] Czech Technical University, Prague, Brehová 7, 11519 Prague 1, Czech Republic
[r] Institute of Physics and Technology, University of Bergen, Allégaten 55, 5007 Bergen, Norway
[s] Department of Physics, University of Oslo, Sem Sælandsvei 24, 0371 Oslo, Norway
[t] Stefan Meyer Institute for Subatomic Physics, Austrian Academy of Sciences, Boltzmanngasse 3, 1090 Vienna, Austria
[u] Joint Institute for Nuclear Research, 141980 Dubna, Russia
[v] INFN Padova, via Marzolo 8, 35131 Padova, Italy
[w] Institute of Nuclear Physics, CNRS/IN2p3, University of Lyon 1, 69622 Villeurbanne, France
[x] University of Bologna, Viale Berti Pichat 6/2, 40126 Bologna, Italy
[y] Department of Physics, University of Pavia, via Bassi 6, 27100 Pavia, Italy
[z] Department of Physics, University of Napoli Federico II, Complesso Universitario di Monte S. Angelo, 80126 Napoli, Italy

* Corresponding author.
  E-mail address: sebastiano.mariazzi@cern.ch (S. Mariazzi).

ABSTRACT

We describe a system designed to re-bunch positron pulses delivered by an accumulator supplied by a positron source and a Surko-trap. Positron pulses from the accumulator are magnetically guided in a 0.085 T field and are injected into a region free of magnetic fields through a μ-metal field terminator. Here positrons are temporally compressed, electrostatically guided and accelerated towards a porous silicon target for the production and emission of positronium into vacuum. Positrons are focused in a spot of less than 4 mm FWTM in bunches of ~8 ns FWHM. Emission of positronium into the vacuum is shown by single shot positron annihilation lifetime spectroscopy.
© 2015 CERN for the benefit of the Authors. Published by Elsevier B.V. This is an open access article under the CC BY license (http://creativecommons.org/licenses/by/4.0/).

1. Introduction

In the last decade the development of an efficient positron trapping and storage technology [1,2] has allowed the production of intense nanosecond-scale positron bunches opening the possibility of new experiments. The use of positron bunching and trapping was at the basis of the first antihydrogen formation [3,4] and the observation of molecular positronium (Ps_2) [5].

Fields that have benefitted from this technique are positronium (Ps) spectroscopy [6,7] and Ps–Ps interaction studies [8] thanks to the high yield of positronium in vacuum that can be obtained by accelerating positron bursts to hit porous silica materials.

Ps is a purely leptonic atom consisting of an electron and its antiparticle, the positron (e^+). Ps can exist in the singlet state, parapositronium (p-Ps, total spin 0, formation probability 1/4) or in the triplet state, orthopositronium (o-Ps, total spin 1, formation probability 3/4). In vacuum, p-Ps decays into 2γ rays with a mean lifetime of 125 ps, while o-Ps decays into 3γ rays with a mean lifetime of 142 ns.

The production of dense Ps clouds in vacuum is also critical to perform many other fundamental experiments such as the production of antihydrogen through charge exchange reactions between antiprotons and Ps excited into Rydberg states [9–11], precise spectroscopy experiments for QED tests [12–14], tests of gravity on matter–antimatter systems [15], high resolution tests for the existence of mirror matter [16] and tests of laser cooling on ultra-light atoms [17].

In this paper, we present the commissioning tests performed with an apparatus designed and built to re-bunch pulses of $10^7 – 10^8$ positrons [18] dumped from the Surko-type accumulator of the AEgIS experiment (Antimatter Experiment: gravity, Interferometry, Spectroscopy) [10,19,20] at CERN.

The exit of the AEgIS Surko system is split into two different beam lines for two different purposes (Fig. 1): the first one is dedicated to inject bunched positrons into the experiment main magnets, while the second one supplies bunched positrons to the re-bunching apparatus. The latter has been developed and installed in order to optimize the use of the bunched positron beam by performing Ps spectroscopy experiments when e^+ are not requested by the main AEgIS experiment. Unlike other similar devices [21], here positrons are extracted from a strong magnetic field by appropriate electrodes that also compress in time, transport and focus the positron cloud on a grounded target. Ps is produced and emitted into vacuum by implanting the positron bunch with a tuneable energy of several keV on a suitable converter. The apparatus is designed to produce Ps in a region with a magnetic field tunable from less than 2 Gauss up to 300 Gauss, which allows one to perform spectroscopic experiments that require various environmental conditions (see for example Refs. [22,23]).

In Section 2, the AEgIS Surko apparatus is described, while in the following one the positron re-bunching system is presented. Sections 3 and 4 are devoted to the description of the performances of the buncher with regards to time compression and focusing of positrons on the target, respectively. Finally, emission of a dense Ps cloud from nanochannelled samples is shown by single shot positron annihilation lifetime spectroscopy (SSPALS) in Section 5.

2. Positron accumulator and e^+ dump production

In the present system (see Fig. 1), positrons are produced via β^+ decay by a ^{22}Na source with an activity of around 11 mCi. A solid Ne moderator is used to slow down fast positrons from the radioactive source down to an energy of a few eV [24]. The slow e^+ are guided by magnetic fields in the three-stage Surko-trap (First Point scientific technology) [2]. The combined efficiency of moderation and transport has been estimated to be ~ $2.5 \cdot 10^{-3}$ [19]. In the Surko-trap the positrons are cooled by interacting with N_2 gas, and released after trapping every 0.15 s with an energy of 17 eV. The number of positrons in each bunch has been measured to be between 2.5 and $3 \cdot 10^4$. The trapping/dumping efficiency is 0.14, calculated as the ratio between positrons injected in the trap and positrons dumped from the trap [19]. Positrons released from
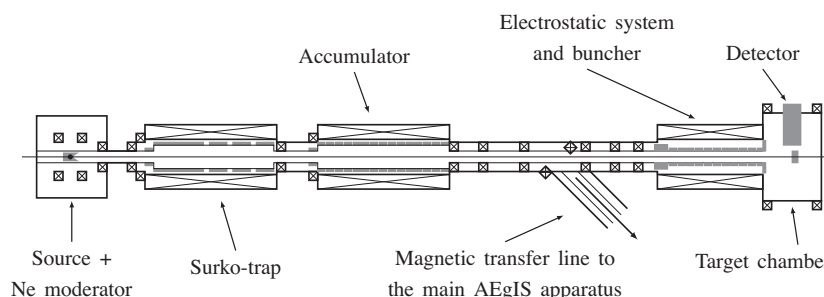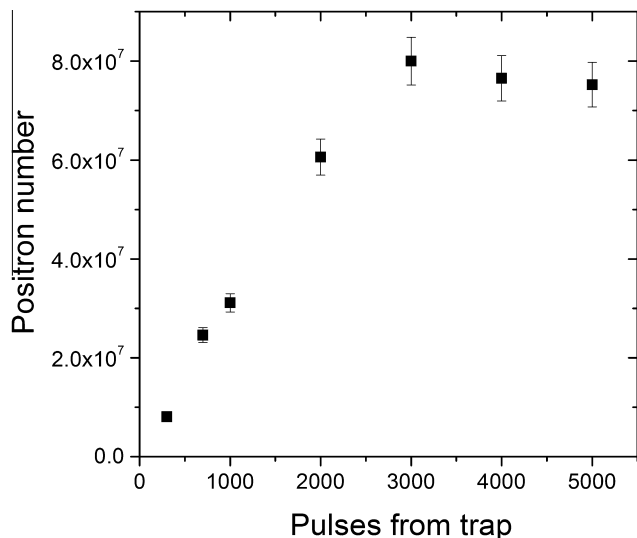

Fig. 1. Sketch of the AEgIS positron system.

Fig. 2. Number of positrons in the accumulator plotted against the number of pulses from the Surko-trap. Source intensity of 11 mCi. The signal was acquired with a calibrated CsI detector coupled to a photodiode. Only statistical errors are shown.

Fig. 3. Sketch of the electrostatic system (a) and simulation of positron bunching and focusing from the end of magnetic section to the target performed with the SIMION® 8 code (b).

the trap are magnetically transported to the accumulator where many positron pulses can be stored for several hundreds of seconds, due to a low base pressure (low 10^{-10} mbar).

The e^+ radial confinement in the accumulator is guaranteed by a 0.1 T magnetic field generated by a homogeneous solenoid ($\Delta B/B \sim 10^{-4}$). Longitudinal confinement of the positrons is ensured by a harmonic potential well approximately 14 V deep generated by 23 electrodes of 2.54 cm in diameter. The total length of the trap is around 23 cm and the central electrode is segmented into four sections in order to apply a rotating electric field for compression of the positron plasma [25]. A potential of 360 mV and a frequency of 5.3 MHz was used in the tests presented here.

Fig. 2 shows the number of positrons stored in the accumulator as a function of the number of pulses from the trap (and thus as a function of time). Up to $8 \cdot 10^7$ positrons can be stored in around 450 s (corresponding to roughly 3000 pulses from the trap). This test was performed by storing positrons for a given time and then dumping the e^+ by raising a potential with its maximum amplitude tunable from a few tens of eV up to around 400 eV. Dumped positrons annihilated on a stopper placed at the exit of the accumulator and the emitted annihilation gamma rays were detected by a calibrated CsI detector coupled to a photodiode, in order to determine the absolute positron number.

The bunching system described in the present paper has been designed to work with positrons dumped from the accumulator with an energy of around 100 eV. The positron bunch at the exit of the accumulator has a typical temporal FWHM of about $15 - 20$ ns [21].

3. Electrostatic transport and positron re-bunching

Positrons dumped from the accumulator are magnetically transported along a distance of ~60 cm by six solenoidal coils generating a maximum magnetic field of 0.14 T and then injected into a series of 28 electrodes (Fig. 3a) designed to [18]:

1. extract the positrons from the magnetic field and guide them towards the target chamber, where a field free zone is required for several Ps experiments,
2. accelerate positrons to implant them in the target (kept at ground potential) with energies up to several keV,
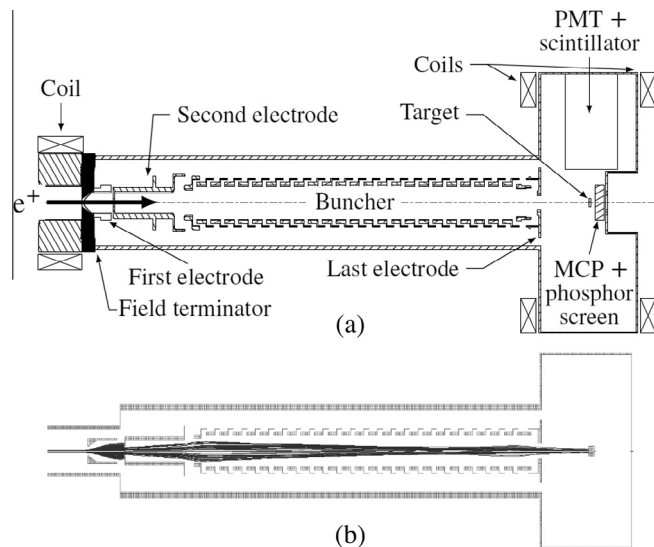
3. focus the positron cloud on the target with a spot smaller than 5 mm and with a time spread of less than 9 ns.

The electro-optical transport, bunching and focusing was simulated from the output of the accumulator to the target position with the SIMION® 8 code (Fig. 3b) [26]. The first electrode (see Fig. 3a) is made of μ-metal and with the supporting flange acts as a magnetic field terminator to reduce the field from 0.085 T (the transport magnetic field immediately before the injection in the electrostatic system) to 0.02 T within 5 mm [27]. The μ-metal electrode, at -800 V, the second electrode (-2100 V) and the following 25 electrodes of the buncher (initially held at -535 V) form two lenses focusing the positrons into the middle of the buncher itself.

The buncher, composed of 25 electrodes of 1.6 cm, has a total length of 40 cm, thus containing the entire positron pulse which, at the buncher entrance, is ~20 cm long according to the simulations. When the positron pulse enters the buncher, a parabolic potential is raised between the first and the last electrode in order to compress the pulse in time and space [18]. The parabolic
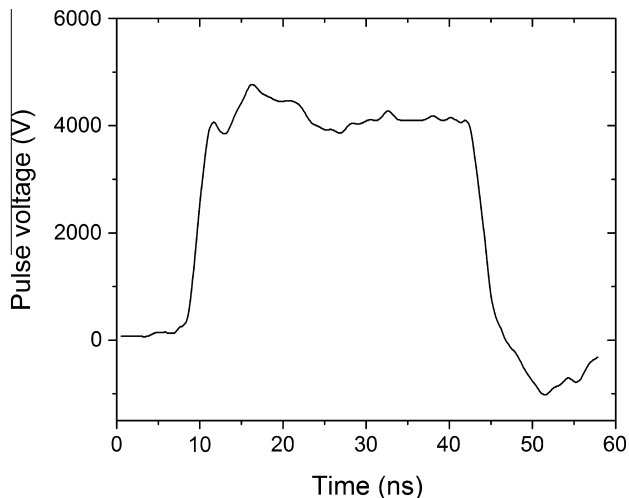
Fig. 4. Shape of the high voltage pulse as a function of time acquired at the input of the buncher, measured with a Magnelab CT-C1.0 current transformer.

function of variable amplitude is superimposed to a tunable bias in order to accelerate the positrons towards the target. The total voltage (parabolic amplitude + bias) is generated by a customized $4 - 10$ kV HV power supply (FID GmbH technology, model FPG 10–003NM30) with a pulse duration of 30 ns and a rise time of $2 - 3$ ns (Fig. 4).

The following tests were performed with a parabolic amplitude of 900 V and a bias voltage of 3300 V, corresponding to a high voltage pulse of 4200V. A last electrode, held at -3000 V, was placed downstream of the buncher and used to focus the beam on the target kept at ground potential 5.6 cm away from the last electrode.

## 4. Buncher synchronization and positron compression

A digital delay generator (Stanford Research Systems DG 645) was used to synchronize the buncher's pulse with the posi-trons dumped from the accumulator. A fast detector with a PbF_2 crystal (diameter 20 mm, length 60 mm) coupled to a Hamamatsu R11265–100 PMT was placed at 4 cm from the target to detect the gamma rays generated by the annihilation of the transported positrons. The FWHM of the single photon signal was <3 ns. An Al target was used for testing synchronization and positron beam compression.

The signal amplitude of the PbF_2 + PMT detector is shown in Fig. 5 as a function of the time delay between dumping the positrons from the accumulator and the switching-on of the pulser. The time reported on the x-axis of the figure is referred to a time-zero that takes into account the delays due to the trigger of the digital delay generator, the pulser, the electronics of the accumulator and the cables. 1000 pulses from the trap were stored in the accumulator before dumping.

When the parabolic potential in the buncher is switched on too early (time delay <15 ns), the positrons are reflected backwards by the potential wall raised at the entrance of the buncher. As a consequence, the signal from the PMT is around 0 mV. On the other hand, when the pulser is switched on too late (time delay >60 ns), the positrons transit through the buncher without being affected by the high voltage pulse, and the amplitude of the signal is around 40 mV. With a delay of about 20 ns, the signal amplitude is almost three times higher, reaching a value of around 110 mV.
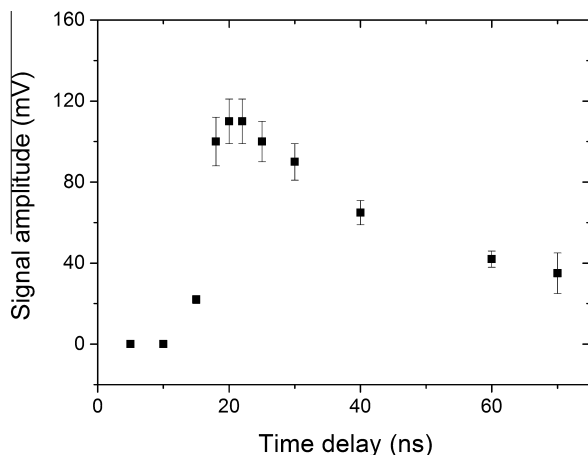
Fig. 5. Signal amplitude from the PbF_2 crystal coupled to a PMT Hamamatsu R11265–100 (see text), as a function of the time delay, when positrons annihilate on an Al target. Each point was measured accumulating 1000 pulses from the trap. For a time delay shorter than 15 ns positrons are reflected. At around 20 ns the signal amplitude is at its maximum because all positrons are inside the buncher when the pulser is switched on, and they are compressed in time (see also Fig. 6). Only statistical errors are given. Where not visible, the error bars are inside the symbols.
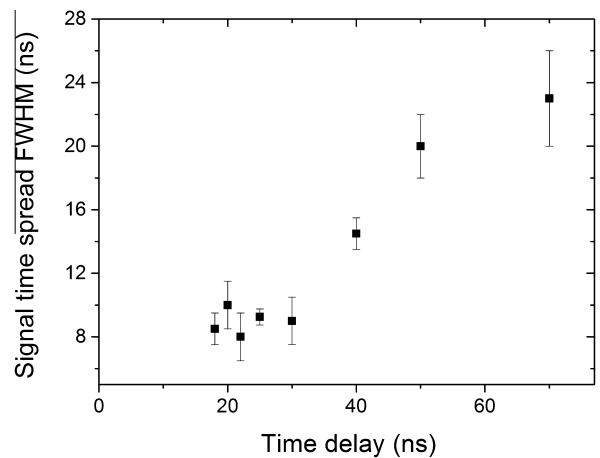
Fig. 6. FWHM of the signal of Fig. 5 vs. time delay. Positron compression occurs for a time delay between 18 and 25 ns. For longer time delays the positrons cross the buncher after the switching on of the high voltage pulse and they are not, or only partially, compressed. Errors are statistical only.
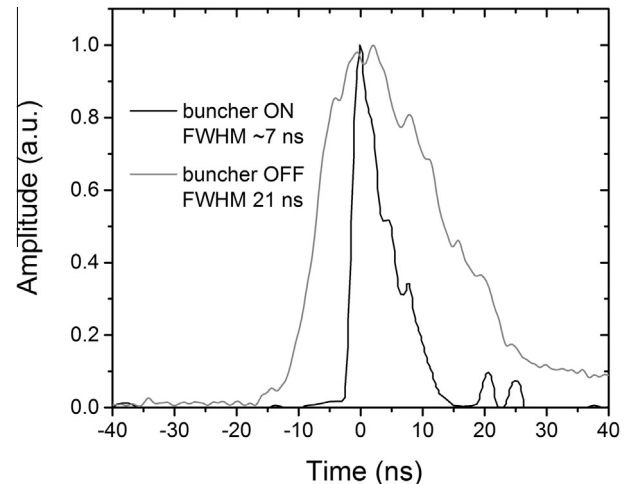

Fig. 7. Comparison of the positron annihilation time distribution on an Al target with the buncher off and buncher on (high voltage pulse of 4200 V). Both signals are normalized to the same amplitude. The FWHM is reduced from 21 ns to ∼7 ns.

The increase of the amplitude with respect to the pass-through configuration is consistent with the compression in time of the positrons. In Fig. 6, the FWHM of the positron annihilation signal is shown as a function of the delay. For a delay longer than 40 ns the FWHM ranges between 15 and 23 ns, showing that the positrons flying through the buncher are not, or only partially, compressed. When the synchronization is adjusted, the signal becomes narrower and, between 18 and 25 ns delay, its width reaches a minimum of around 7–9 ns.

As an example, a comparison of two signals (normalized to the same amplitude) with positron annihilation acquired with the buncher off and on is shown in Fig. 7. With the buncher off the FWHM of the positron annihilation time distribution is around 21 ns, while it decreases to ∼7 ns when the buncher is on.

5. Positron focusing

A microchannel plate (MCP) assembly (Hamamatsu F2222–21P25 + Phosphor Screen P46) was used to characterize the positron spot at the target position. The MCP assembly was placed ∼1 cm behind the target position. The sample holder could be
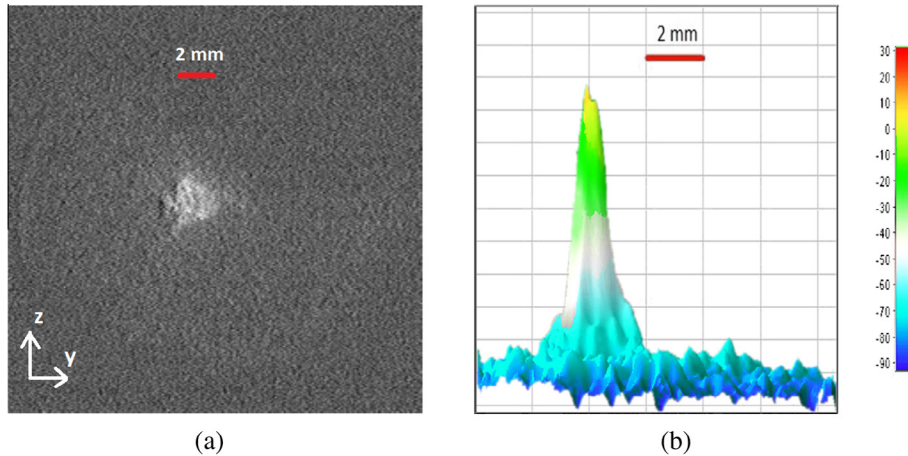
Fig. 8. Positron beam spot acquired with an MCP assembly (a) and corresponding radial intensity distribution (b). The image was recorded with the electrostatic guided positron bunch and no magnetic field in the target region. The FWTM of the positron distribution is <4 mm when positrons are accelerated to an energy of 3.3 keV.
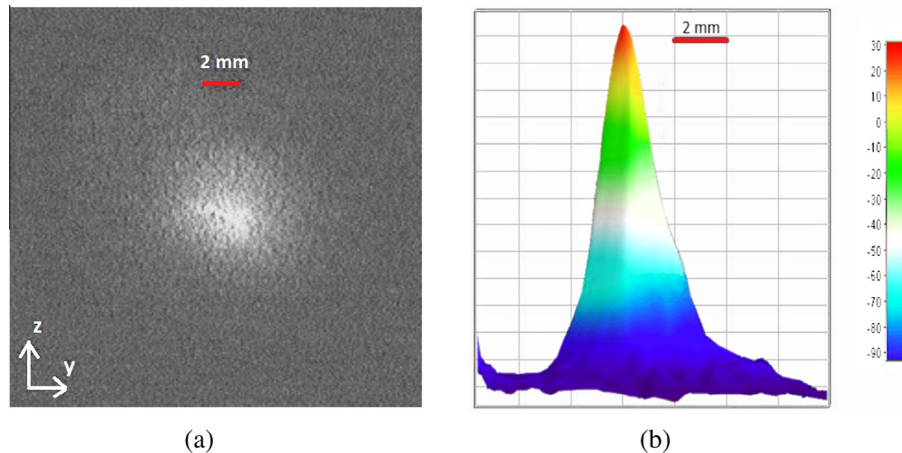
Fig. 9. Positron beam spot acquired with an MCP assembly (a) and corresponding radial intensity distribution (b) when a 250 Gauss field is set in the target region. The FWTM of the positron distribution is around 5 mm when positrons are accelerated to an energy of 3.3 keV.

moved with an actuator in order to dump positrons directly onto the MCP. The positron pulse was imaged on the phosphor screen of the MCP assembly with a charge-coupled device (CCD) camera.

The image of the bunched positron beam on the MCP is shown in Fig. 8(a) when positrons are guided by electrostatic fields and no magnetic field is present in the target chamber. The corresponding intensity distribution is shown in Fig. 8(b).

The FWTM of the spot was found to be smaller than 4 mm. The efficiency of positron extraction from the magnetic field of the transfer line and transport along the buncher has been estimated to be around 30%, using a calibrated CsI detector coupled to photodiodes. Thus, the spot of Fig. 8(a) corresponds to the annihilation of around 10^7 positrons when $3 \cdot 10^7$ positrons are dumped from the accumulator. In this configuration, the magnetic field in the target region has been measured to be below 1.8 Gauss in the direction parallel to the beam and below 0.5 Gauss in the perpendicular direction.

For experiments requiring a specific magnetic field in the target region [22], two coils, generating a field up to 300 Gauss in the direction parallel to the beam, are installed around the target chamber, symmetrically placed with respect to the plane of the target (Fig. 3). When a field higher than 150 Gauss is set, the magnetic field positively affects the extraction of the positrons from the buncher and the fraction of positrons reaching the target increases

up to around 40%. The missing positron fraction is expected to mainly annihilate at the transition between magnetic and electrostatic transport (see simulation in Fig. 3b). The image of the positron beam on the MCP with 250 Gauss in the target region is reported in Fig. 9a) and the corresponding intensity distribution, in Fig. 9(b). In this configuration, the FWTM of the spot is around 5 mm. Taking into account the estimated transport efficiency, the image corresponds to about $1.2 \cdot 10^7$ positrons reaching the target when $3 \cdot 10^7$ positrons are dumped from the accumulator.

6. Positronium formation and detection

A PbWO$_4$ scintillator ($25 \times 25 \times 20$ mm^3) coupled to a Hamamatsu R11265-100 PMT was placed above the sample holder at a distance of 4 cm from the target center. This set-up, which combines a good detection efficiency with a relatively fast time response (FWHM single photon signal around 4 ns), was used to detect the annihilation radiation produced by the intense posi-tron burst and to perform single-shot positron annihilation lifetime spectroscopy [28]. The anode signal from the PMT was divided using a 50 Ω Mini-Circuits ZFRSC-2050B + splitter and was sent into two channels of a Tektronix TDS5054B 500 MHz bandwidth oscilloscope terminated on 50 Ω. One channel, with a vertical scale
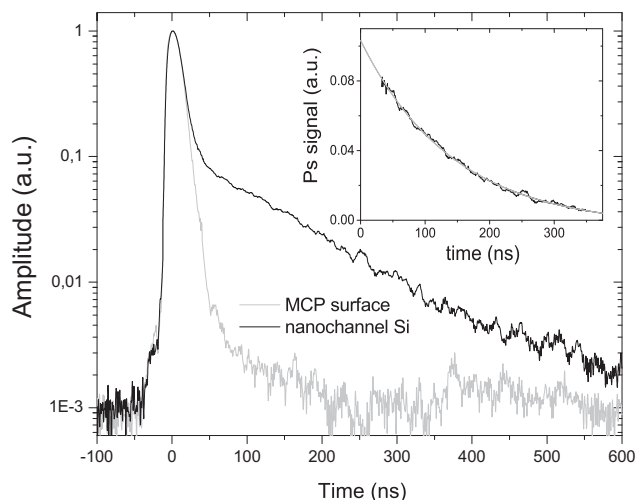
Fig. 10. SSPALS spectra measured on the surface of the MCP (no Ps formation, grey curve) and in a silicon sample with nanochannels (Ps formation, black curve). Each curve is the average of 10 single shots. Positrons were implanted with energy of 3.3 keV. The difference of the two spectra (Ps signal) is shown in the inset. The continuous line is the fit of the experimental curve (see text). The o-Ps lifetime τ from this fit is ~142 ns.

of 1 V/div, was used to acquire the "prompt peak", the other one, with a scale of 100 mV/div, was used to record the low level part of the signal in order to have a low digital noise [29]. Moreover, the high frequency noise of the low gain channel was reduced using a low-pass filter with a cut-off frequency of 100 MHz. The waveforms of the two channels were recorded by a computer and automatically merged to give the SSPALS spectra. Tests of Ps formation and detection were performed by implanting around 10^7 positrons per shot in a silicon sample in which oxidized nanochannels had been electrochemically etched (Fig. 10) [30,31].

The SSPALS obtained by implantation of positrons in the MCP shows a sharp peak corresponding to the fast 2 gamma annihilations of implanted e^+. On the right side of the peak, the signal quickly decreases and reaches the noise level in about 100 ns. On the other hand, the lifetime spectrum measured in the Si sample with nanochannels shows a long tail from ~20 ns up to 600 ns generated by Ps formation and decay. The difference between the two lifetime spectra in the time range 50–350 ns from the prompt peak is reported in the inset of Fig. 10. The continuous line in the graph is the best fit with the exponential function $e^{-(t/\tau)}$ and a constant background term, where t is the time and τ the o-Ps lifetime in vacuum. From this fit $\tau = 142$ ns (with an error of few percent), indicating that the observed o-Ps atoms have a lifetime consistent with emission into vacuum.

From previous characterization of similar positron-positronium converters, around 35% of positrons implanted with an energy of 3300 V are emitted into the vacuum as Ps [30,31]. Thus, when $3 \cdot 10^7$ are dumped from the accumulator, a cloud of about $4 \cdot 10^6$ positronium atoms emitted into vacuum can be estimated by using the Ps diffusion model of Ref. [30].

7. Conclusion

A new apparatus designed to provide intense positron bunch-es for the production of positronium into vacuum has been tested. The system, using a 11 mCi source, allows for the compression of around 10^7 positrons in a bunch with a FWHM of around 8 ns and a spot size of less than 4 mm FWTM. The use of a μ-metal field terminator and the subsequent electrostatic transport permitted us to extract positrons from the magnetic field of the AEgIS positron

transport line and to guide them to an e^+/Ps converter placed in a region free of magnetic fields. Efficient formation and emission into vacuum of ground state o-Ps (around 35%) have been demonstrated with SSPALS measurements. The apparatus is installed in proximity of the AEgIS laser system [32]. UV and IR laser beams can easily be guided and injected into the target chamber, where they are being used for several experiments on o-Ps spectroscopy, such as n=3 excitation and o-Ps Rydberg atoms production.

References

[1] T.J. Murphy, C.M. Surko, Positron trapping in an electrostatic well by inelastic collisions with nitrogen molecules, Phys. Rev. A 46 (1992) 5696.
[2] J.R. Danielson, D.H.E. Dubin, R.G. Greaves, C.M. Surko, Plasma and trap-based techniques for science with positrons, Rev. Mod. Phys. 87 (2015) 247.
[3] M. Amoretti et al., (ATHENA collaboration), Production and detection of cold antihydrogen atoms, Nature 419 (6906) (2002) 456.
[4] G. Gabrielse et al., (ATRAP collaboration), Background-free observation of cold antihydrogen with field-ionization analysis of its states, Phys. Rev. Lett. 89 (21) (2002) 213401.
[5] D.B. Cassidy, A.P. Mills Jr, The production of molecular positronium, Nature 449 (7159) (2007) 195.
[6] D.B. Cassidy, T.H. Hisakado, H.W.K. Tom, A.P. Mills Jr, Efficient production of Rydberg positronium, Phys. Rev. Lett. 108 (4) (2012) 043401.
[7] D.B. Cassidy, T.H. Hisakado, H.W.K. Tom, A.P. Mills Jr, Optical spectroscopy of molecular positronium, Phys. Rev. Lett. 108 (13) (2012) 133402.
[8] D.B. Cassidy, A.P. Mills Jr, Enhanced Ps–Ps interactions due to quantum confinement, Phys. Rev. Lett. 107 (21) (2011) 213401.
[9] M. Charlton, Antihydrogen production in collisions of antiprotons with excited states of positronium, Phys. Lett. A 143 (3) (1990) 143.
[10] M. Doser et al., (AEgIS collaboration), Exploring the WEP with a pulsed cold beam of antihydrogen, Classical Quantum Gravity 29 (18) (2012) 184009.
[11] P. Debu et al., (GBAR collaboration), Gbar, Hyperfine Interact. 212 (1–3) (2012) 51.
[12] M.S. Fee, S. Chu, A.P. Mills Jr, R.J. Chichester, D.M. Zuckerman, E.D. Shaw, K. Danzmann, Measurement of the positronium $1^3S_1 - 2^3S_1$ interval by continuous-wave two-photon excitation, Phys. Rev. A 48 (1) (1993) 192.
[13] F. Castelli, I. Boscolo, S. Cialdi, M.G. Giammarchi, D. Comparat, Efficient positronium laser excitation for antihydrogen production in a magnetic field, Phys. Rev. A 78 (5) (2008) 052512.
[14] D.B. Cassidy, T.H. Hisakado, H.W.K. Tom, A.P. Mills Jr, Positronium hyperfine interval measured via saturated absorption spectroscopy, Phys. Rev. Lett. 109 (7) (2012) 073401.
[15] D.B. Cassidy, S.D. Hogan, Atom control and gravity measurements using Rydberg positronium, International Journal of Modern Physics: Conference Series, vol. 30, World Scientific, 2014, p. 1460259.
[16] P. Crivelli, A. Belov, U. Gendotti, S. Gninenko, A. Rubbia, Positronium portal into hidden sector: a new experiment to search for mirror dark matter, J. Instrum. 5 (08) (2010) P08001.
[17] T. Kumita, T. Hirose, M. Irako, K. Kadoya, B. Matsumoto, K. Wada, N.N. Mondal, H. Yabu, K. Kobayashi, M. Kajita, Study on laser cooling of ortho-positronium, Nucl. Instr. Meth. Phys. Res. Sect. B 192 (1) (2002) 171.
[18] L. Penasa, L. Di Noto, M. Bettonte, S. Mariazzi, G. Nebbia, R.S. Brusa, Positron bunching system for producing positronium clouds into vacuum, Journal of Physics: Conference Series, vol. 505, IOP Publishing, 2014, p. 012031.
[19] S. Mariazzi et al., (AEgIS collaboration), AEgIS experiment: towards antihydrogen beam production for antimatter gravity measurements, Eur. Phys. J. D 68 (3) (2014) 41.
[20] S. Aghion et al., (AEgIS collaboration), Prospects for measuring the gravitational free-fall of antihydrogen with emulsion detectors, J. Instrum. 8 (08) (2013) P08013.

[21] D.B. Cassidy, S.H.M. Deng, R.G. Greaves, A.P. Mills Jr, Accumulator for the production of intense positron pulses, Rev. Sci. Instrum. 77 (7) (2006) 073106.

[22] F. Castelli, The positronium atom as a benchmark for Rydberg excitation experiments in atomic physics, Eur. Phys. J. Spec. Top. 203 (2012) 137.

[23] T.E. Wall, A.M. Alonso, B.S. Cooper, A. Deller, S.D. Hogan, D.B. Cassidy, Selective production of Rydberg-Stark states of positronium, Phys. Rev. Lett. 114 (17) (2015) 173001.

[24] A.P. Mills Jr, E.M. Gullikson, Solid neon moderator for producing slow positrons, Appl. Phys. Lett. 49 (17) (1986) 1121.

[25] C.M. Surko, R.G. Greaves, Emerging science and technology of antimatter plasmas and trap-based beams, Phys. Plasmas 11 (5) (2004) 2333.

[26] Scientific Instrument Services (SIS), Simion. URL: <http://simion.com>

[27] L. Di Noto, Positronium in AEgIS experiment: study on its emission from nanochanneled samples and design of a new apparatus for Rydberg excitations (Ph.D. dissertation), University of Trento, Italy, 2014. URL: <http://eprints-phd.biblio.unitn.it/1149/1/tesi_PhD.pdf>.

[28] D.B. Cassidy, A.P. Mills Jr, A fast detector for single-shot positron annihilation lifetime spectroscopy, Nucl. Instr. Meth. Phys. Res. Sect. A 580 (3) (2007) 1338.

[29] D.B. Cassidy, S.H.M. Deng, H.K.M. Tanaka, A.P. Mills Jr, Single shot positron annihilation lifetime spectroscopy, Appl. Phys. Lett. 88 (19) (2006) 194105.

[30] S. Mariazzi, P. Bettotti, S. Larcheri, L. Toniutti, R.S. Brusa, High positronium yield and emission into the vacuum from oxidized tunable nanochannels in silicon, Phys. Rev. B 81 (23) (2010) 235418.

[31] S. Mariazzi, P. Bettotti, R.S. Brusa, Positronium cooling and emission in vacuum from nanochannels at cryogenic temperature, Phys. Rev. Lett. 104 (24) (2010) 243401.

[32] S. Cialdi, I. Boscolo, F. Castelli, F. Villa, G. Ferrari, M.G. Giammarchi, Efficient two-step positronium laser excitation to Rydberg levels, Nucl. Instr. Meth. Phys. Res. Sect. B 269 (13) (2011) 1527.